JOURNAL OF MOLECULAR SPECTROSCOPY 138, 89–101 (1989)

The HF and DF $B^1\Sigma^+ - X^1\Sigma^+$ and $C^1\Pi - X^1\Sigma^+$ Band Systems Studied by 1 XUV + 1 UV Resonance Enhanced Multiphoton Ionization

LYNN M. TASHIRO, WIM UBACHS,[1] AND RICHARD N. ZARE

Department of Chemistry, Stanford University, Stanford, California 94305

Rotationally resolved spectra of the HF and DF $C^1\Pi - X^1\Sigma^+$ and $B^1\Sigma^+ - X^1\Sigma^+$ band systems are recorded in the wavelength range 93.8–99.0 nm by 1 XUV + 1 UV resonance enhanced multiphoton ionization (REMPI). Spectroscopic constants for the HF and DF $C^1\Pi$ $v = 0$ states and for a sequence of 14 vibrational levels of DF $B^1\Sigma^+$ are determined. The $B^1\Sigma^+$ state is found to be perturbed by the $C^1\Pi$ and $D^1\Sigma^+$ states, as previously reported. XUV + UV REMPI is shown to be a viable method for state selective detection of HF with a detection sensitivity of 10^7 molecules per cm^3 per quantum state. © 1989 Academic Press, Inc.

1. INTRODUCTION

The main features of the hydrogen halide electronic structure were discussed by Mulliken in a pair of classic papers (*1, 2*). Confirming the predicted existence of a widely bound valence state with ionic character, Johns and Barrow (*3*) and, later, DiLonardo and Douglas (*4*) observed a long progression of vibrational bands in the vacuum ultraviolet. In the latter work vibrational levels up to $v' = 73$ were identified for the HF $B^1\Sigma^+$ state, which was formerly denoted as $V^1\Sigma^+$ by Mulliken. The correct vibrational assignment of this long progression could be derived from analysis of $B^1\Sigma^+ v = 0$–10–$X^1\Sigma^+ v = 7$–19 VUV emission data and from $B^1\Sigma^+ v = 14$–73–$X^1\Sigma^+ v = 0$ XUV absorption data (*4*). In order to establish the correct position of the vibrational energy levels of the $B^1\Sigma^+$ state relative to the $v = 0$ level of the ground state, information derived from infrared emission data (*5, 6*) was included in the analysis. More recently, Douglas and Greening (*7*) reported observation of transitions to the HF $C^1\Pi$ and $b^3\Pi$ Rydberg states in the wavelength range $\lambda < 100$ nm. For DF, the available spectroscopic information is more limited than that for HF. The rotational constants for the $X^1\Sigma^+$ ground state (*8*) and the $C^1\Pi$ Rydberg state (*7*) are well established, but the $B^1\Sigma^+$ state is only analyzed for the lowest six vibrational levels $v = 0$–5 (*3, 9*).

This paper presents a reexamination of electronically excited HF and DF via high-resolution, two-color resonance enhanced multiphoton ionization (REMPI) spectroscopy. In this technique the rovibronic levels of the HF or DF $B^1\Sigma^+$ and $C^1\Pi$ states are resonantly excited by absorption of one XUV photon at frequencies in excess of

[1] Present address: Natuurkundig Laboratorium, Vrije Universiteit, De Boelelaan 1081, Amsterdam, The Netherlands.

0022-2852/89 $3.00

100 000 cm^{-1} (below the lithium fluoride wavelength cutoff at 105 nm). Subsequent absorption of one additional UV photon causes ionization of the excited molecule. The mass-selected ion signal is collected as a function of the XUV wavelength to generate rotationally resolved spectra of the $B^1\Sigma^+ - X^1\Sigma^+$ and $C^1\Pi - X^1\Sigma^+$ transitions. The present work gives the first account of XUV absorption to higher vibrational levels of the DF $B^1\Sigma^+$ state in the energy range 100 000–106 000 cm^{-1}. The spectral accuracy of our laser-based XUV spectrometer is an order of magnitude higher than that of previous studies that used photographic techniques. This permits the extraction of more refined molecular constants.

2. EXPERIMENTAL DETAILS

The XUV spectrometer is the same as previously described in the 1 + 1 REMPI studies of N_2 (*10*). XUV radiation is produced by third harmonic generation in a pulsed jet of atomic or molecular gas. The frequency-doubled output of a Nd:YAG pumped-dye laser (Quanta-Ray DCR1A/PDL 1) at λ = 280–300 nm is focused by a 25-cm lens 1 mm below the orifice of a pulsed nozzle (Lasertechnics LPV) producing XUV with efficiency on the order of 10^{-6} (*11*). For the production of XUV radiation in the range 93–100 nm, xenon is used as the tripling gas (*11*). Over a small wavelength range, 95.0–95.5 nm, N_2 was used as the tripling medium because its third harmonic conversion efficiency in this range is an order of magnitude higher than that of Xe (*12*). Fortunately, this range coincides with the HF and DF C–X (0, 0) bandheads.

The dye laser is equipped with an intracavity etalon (Molectron) resulting in a bandwidth of 0.03–0.05 cm^{-1} in the visible and energies of 5–7 mJ/pulse in the UV. The wavelength is scanned by pressure tuning the cavity with CO_2, allowing for continuous scans of 10 cm^{-1} in the visible, which corresponds to 60 cm^{-1} in the XUV (generated by frequency tripling the doubled output of the dye laser). The residual visible light is separated from the UV by a dichroic mirror and is used for calibration purposes. The iodine absorption spectrum in the visible (*13, 14*) and the transmission fringes from a solid etalon are recorded simultaneously with the ion spectrum on a three-pen chart recorder.

The copropagating, diverging XUV/UV beams are directed into a differentially pumped sample chamber. HF or DF is introduced into the chamber through either a second pulsed nozzle (General Valve) or an adjustable leak valve. Because of the corrosive nature of HF and DF, the gases could not be used in their pure state. Mixtures of 15–30% HF or DF in Ar or He were used to obtain our data. The base pressure of the sample chamber was 5×10^{-7} torr. The adjustable leak valve was used to measure the HF detection sensitivity of our apparatus. The spectroscopic data were obtained using the pulsed nozzle operated with 15–30 psi backing pressure located 2.25 in. from the laser beam. The HF/DF is ionized in the region between a pair of repeller and extractor plates (2 in. in diameter and 1 in. apart) with typical static voltages of V_R = 1500 V and V_E = 800 V. The nascent ions are accelerated through a slit in the extractor plate into a 60-cm time-of-flight (TOF) chamber where they are detected on a two-layer multichannel detector (Galileo MCP-B-25).

3. RESULTS AND DISCUSSION

A. Spectra

Figure 1 and Fig. 2 present a typical overview spectrum for HF and DF molecules in the wavelength range 94.4–95.4 nm. For these spectra the dye laser is operated without an intracavity etalon; consequently, the observed spectral linewidth of 1.5 cm^{-1} can be attributed predominantly to the linewidth of the sextupled dye laser.

Xenon was used as the tripling gas. Figure 3 shows the relative XUV production for Xe in a region where HF and DF were studied. The spectrum has been normalized for input UV power and the technique by which it was measured is described elsewhere (*15*). The peaks in the tripling efficiency are caused by dips in the absorption coefficient of Xe (*16, 17*). Each minimum coincides with an autoionization resonance from either the $5p$-ns' or $5p$-nd' Rydberg series. The exponential loss caused by absorption at the third harmonic dominates any resonant enhancement of the third order susceptibility, $\chi^{(3)}$. Relative intensities of the HF and DF rotational transitions reflect the varying XUV power as well as relative rotational state populations.

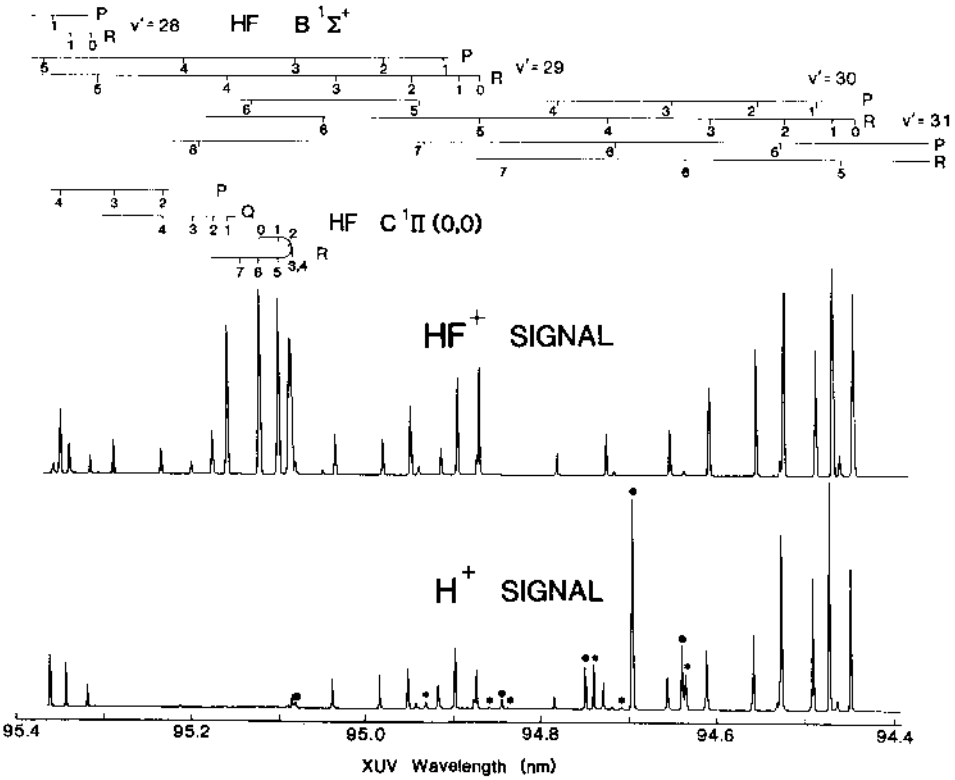

FIG. 1. Typical overview spectrum of HF, measured by mass-selected 1 + 1 REMPI. The upper trace represents the HF^+ signal, the lower trace the H^+ signal. Lines marked with solid circle or an asterisk are from H_2 impurities and arise from $B^1\Sigma_u^+$–$X^1\Sigma_g^+$ and $C^1\Pi_u$–$X^1\Sigma_g^+$ transitions of H_2, respectively.

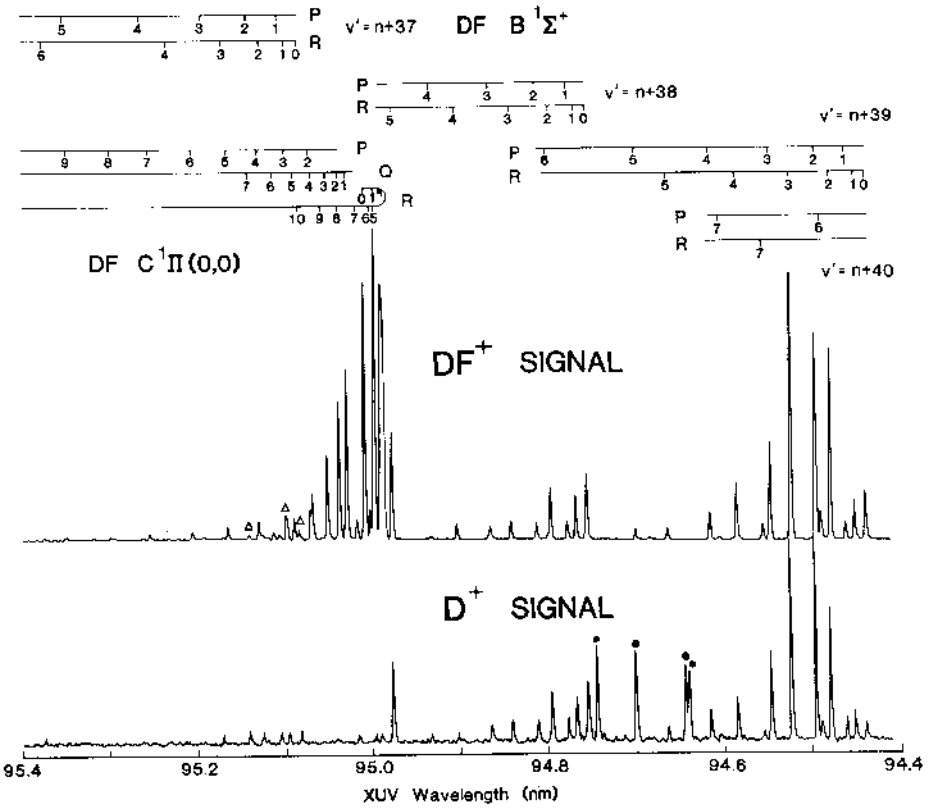

FIG. 2. Typical overview spectrum of DF, measured by mass-selected 1 + 1 REMPI. The upper trace represents the DF^+ signal, the lower trace the D^+ signal. Lines marked with a solid circle or an asterisk arise from $B^1\Sigma_u^+$–$X^1\Sigma_g^+$ and $C^1\Pi_u$–$X^1\Sigma_g^+$ transitions of H_2, respectively. Lines marked with a Δ represent overlapped $C^1\Pi$–$X^1\Sigma^+$ and $B^1\Sigma^+$–$X^1\Sigma^+$ DF transitions.

All spectral features in Fig. 1 can be assigned as resulting from one-photon XUV absorptions, corresponding to transitions from the HF $X^1\Sigma^+ v = 0$ ground state to the HF $C^1\Pi$ $v = 0$ and HF $B^1\Sigma^+ v = 28$, 29, 30, and 31 excited states. HF^+ and H^+

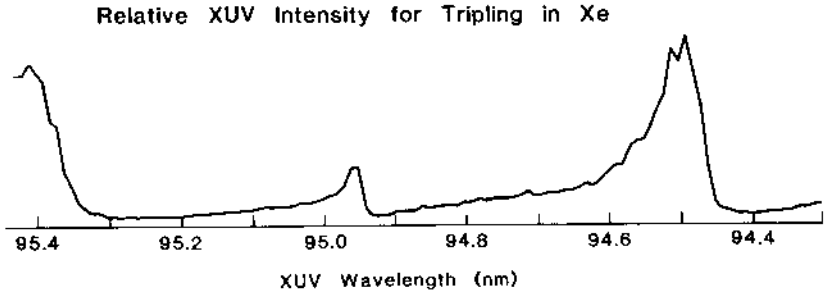

FIG. 3. Relative XUV output power using Xe as the tripling medium. Structure in the efficiency is caused by autoionization resonances in the XUV.

ions are produced by subsequent absorption of UV photons. Ion yields at mass 1 (H^+) and mass 20 (HF^+) are separated in the TOF setup and recorded simultaneously. H^+ and H_2^+ are also produced by 1 + 1 MPI of H_2 through the $B^1\Sigma_u^+$–$X^1\Sigma_g^+$ and $C^1\Pi_u$–$X^1\Sigma_g^+$ transitions, where the H_2 is a background contaminant. These transitions through the H_2 B and C states are denoted by solid circles and asterisks, respectively, in Fig. 1.

Similarly all spectral features in Fig. 2 can be assigned as resulting from one-photon XUV absorptions corresponding to transitions from the DF $X^1\Sigma^+ v = 0$ ground state to the DF $C^1\Pi$ $v = 0$ and DF $B^1\Sigma^+ v = n + 37$, $n + 38$, $n + 39$, and $n + 40$ excited states. D^+ has the same charge to mass ratio as H_2^+, hence the lower trace of Fig. 2 contains H_2^+ signals again from the 1 + 1 MPI of the H_2 contaminant. These transitions are also labeled by solid circles and asterisks for excitations through the B and C states. All the ions are produced in 1 XUV + 1 UV processes, since 3 + 1 UV REMPI processes cannot take place in a configuration with nonfocused UV radiation. Signals are found to be completely dependent on the generation of the third harmonic in the pulsed jet of xenon.

Accurate positions of single rotational lines were determined from 1 + 1 REMPI spectra taken with an air-spaced etalon inserted in the dye laser (see Fig. 4). The convolution of the Doppler width of HF (DF), 0.3 cm^{-1}, with the bandwidth of the XUV radiation, 0.12 cm^{-1}, is 0.32 cm^{-1}. Observed linewidths ranged from 0.39 to 1.54 cm^{-1}. The resolution is comparable, but the accuracy achieved here is an order of magnitude better than previous nonlaser XUV absorption studies (*3, 4, 7*). A spectrum taken with the etalon of the (0, 0) bandhead portion of the DF $C^1\Pi$–$X^1\Sigma^+$ transition is shown in Fig. 4. The absolute calibration of the wavelength, which is a general problem in XUV spectroscopy, was carried out by a simultaneous measurement of the iodine absorption spectrum at the fundamental laser wavelength. Interpolation between the dense I_2 lines (*13, 14*) allows for a determination of the absolute HF and DF line positions within 0.05 cm^{-1} in the XUV.

For HF, a portion of the observed spectral lines was assigned in previous XUV absorption studies by DiLonardo and Douglas (*4*) and by Douglas and Greening (*7*). Identification of rotational lines in the energy range around 105 000 cm^{-1} is hampered by the near coincidences of transitions to several vibrational states of the HF $B^1\Sigma^+$, the HF $C^1\Pi$ state, and the HF $b^3\Pi$ state, the last being observed only weakly in our experiment. In transitions to the HF $C^1\Pi$ state, the H^+ yield is very low or absent. This facilitated assignment of the correct quantum numbers. Differences in the spectra, measured at different masses in the TOF setup (masses 2 and 21 for DF), could be used to determine accurate line positions of blended lines. For example, the contribution at mass 21 of the $P(2)$ transition in the DF B–X ($n + 37$, 0) band was also measured at mass 2. This allowed deconvolution from the $Q(7)$ transition of the DF C–X (0, 0) band, which does not contribute to a signal at mass 2.

The spectra of the HF and DF C–X and B–X transitions are severely perturbed by mutual interactions between the B and C states. The observed HF and DF $C^1\Pi$–$X^1\Sigma^+$ line positions are given in Table I. By symmetry, the f Λ-doublet components of the $C^1\Pi$ state, which are probed by the Q lines, cannot be affected by the $B^1\Sigma^+$ state. The Q lines were fit in a least-squares manner to Hamiltonians of the form

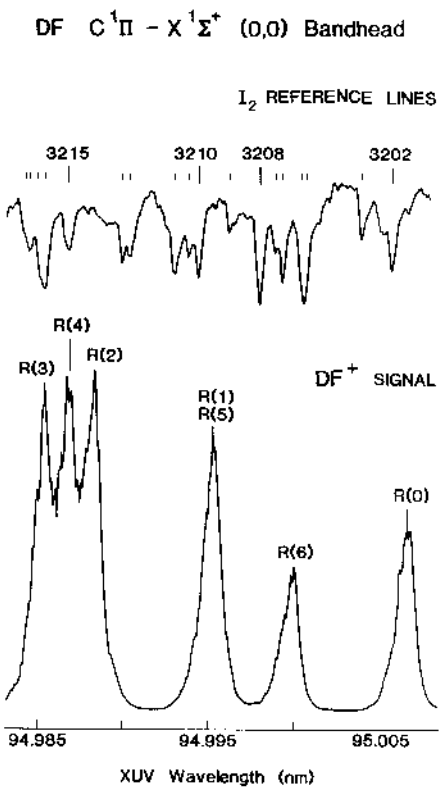

FIG. 4. Spectrum of DF measured using the intracavity etalon by mass-selected 1 + 1 REMPI. The upper trace refers to the I_2 absorption spectrum recorded as an absolute frequency calibration (see text). The lower trace shows the DF $C^1\Pi$–$X^1\Sigma^+$ (0, 0) bandhead region, recorded at mass 21 (DF^+).

$$H = B_v[J(J+1) - \Lambda^2] - D_v[J(J+1) - \Lambda^2]^2 \qquad (1)$$

for the $C^1\Pi$ and $X^1\Sigma^+$ states. Data from Ref. (*7*) were included and appropriately weighted in the fit. The rotational constants for the ground state were fixed at the very accurate values of Jennings and Wells (*18*) for HF (B_0 = 20.5597300 cm^{-1} and D_0 = 2.11991 × 10^{-3} cm^{-1}) and of DeLucia, Helminger, and Gordy (*8*) for DF (B_0 = 10.86035 cm^{-1} and D_0 = 5.884 × 10^{-4} cm^{-1}). The molecular constants for the C state from the least-squares fit are given in Table II. Indeed, a fit of only the Q-branch lines yields constants that result in good agreement between observed and calculated values. The D_0 value for the HF $C^1\Pi$ state is nominally negative and unphysical. This may indicate either the poor quality of our fit or a slight perturbation, possibly by the HF $b^3\Pi$ state.

The e Λ-doublet components of the $C^1\Pi$ observed via P and R transitions are heavily perturbed. Figure 5 shows that the perturbation between the e Λ-doublet components of the HF and DF $C^1\Pi$ states and the nearby vibrational levels of the HF and DF $B^1\Sigma^+$ states results from a sequence of avoided crossings. The solid curves represent the calculated energy values for the unaffected f Λ-doublet components.

TABLE I

Line Positions (in cm^{-1}) for the HF and DF C–X Band (the Values in the Column for Obs.-Calc. Represent Deviations from a Least-Squares Fit, in Which Only the C–X Q-Branch Transitions (the f Λ-Doublet Component) Are Taken into Account)

	J	R(J)		Q(J)		P(J)	
		observed	obs. -calc.	observed	obs. -calc.	observed	obs. -calc.
HF	0	105 123.09	-0.13				
	1	146.09	-0.16	105 082.05	-0.06		
	2	159.88	-0.47	064.12	-0.03	104 999.79	-0.15
	3	162.54	-3.10	037.37	0.15	940.95	0.00
	4	163.76	1.42	001.54	-0.16	872.96	-0.32
	5	147.94	-2.81	104 957.84	0.04	794.19	-2.97
	6	121.15[a]	-10.0	905.96[a]	0.11	714.40	1.49
	7	096.74	-7.3			618.32	-2.58
	8					511.57	-10.0
	9	007.15	-22.0[b]				
	10	104 987.83	5.3[b]				
DF	0	105 255.59	0.18				
	1	268.23	0.16	105 233.66	-0.03		
	2	276.21	0.03	224.62	-0.03	105 190.85	0.58
	3	279.46	-0.25	211.12	0.04	159.82	0.27
	4	277.80	-0.84	192.88	-0.10	123.58	-0.77
	5	268.23	-4.72	170.66	0.33	084.40	0.27
	6	263.15	0.55	142.92	-0.21	039.70	-0.82
	7	246.78	-0.79	111.33	-0.03	104 987.14	-4.76
	8			074.99	-0.02	939.35	0.55
	9	204.65	1.35	034.29[a]	0.25	880.42	-0.81
	10					815.63	-3.55
	11					753.99	1.34

[a] Line positions are taken from Douglas and Greening (7).

[b] The assignment is uncertain because corresponding P lines were not observed.

For the $B^1\Sigma^+$ vibrational levels, the lines are calculated from molecular constants that were obtained from a fit to transitions to unperturbed low J levels. In all cases, the energy of a perturbed rotational level is pushed away from the crossing point. In both the B and C states, the differences of observed frequencies of $P(J+1)$ and $R(J-1)$ transitions from the calculated unperturbed values agree within the experimental error. For those cases where two transitions, $P(J+1)$ and $R(J-1)$, to the same J level of the e Λ-doublet component for the C state were observed, the assignment is unambiguous, despite the presence of large perturbations.

TABLE II

Molecular Constants (in cm^{-1}) for the HF and DF $C^1\Pi$ $v = 0$ State as Obtained from a Least-Squares Fit, in Which Only the C–X Q-Branch Transitions (the f Λ-Doublet Component) Are Taken into Account (the Cited Uncertainties Represent Two Standard Deviations)

	HF	DF
ν_0	105 107.19 ± 0.08	105 246.81 ± 0.11
B_0	16.03 ± 0.01	8.600 ± 0.008
$D_0 \times 10^4$	-6.5 ± 4.2	6.9 ± 1.0

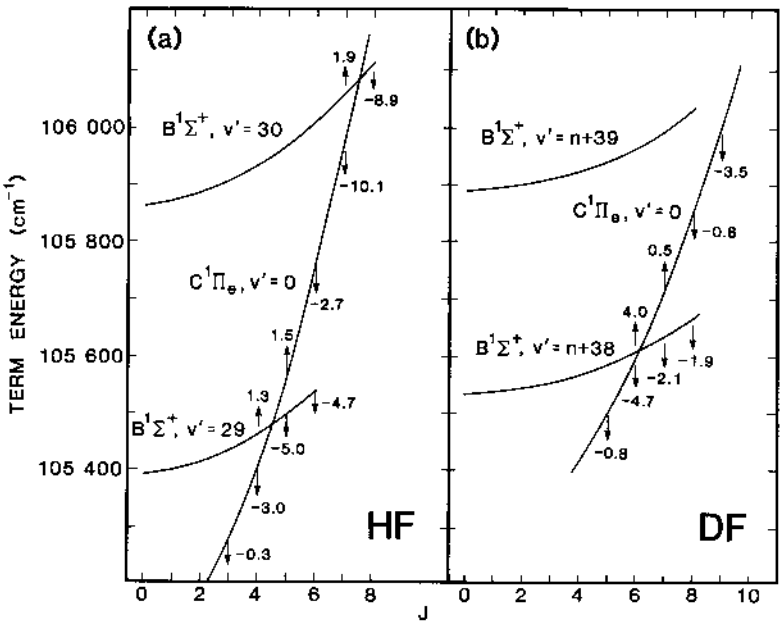

FIG. 5. Perturbations between the HF and DF $B^1\Sigma^+$ and $C^1\Pi$ states. The solid lines represent calculated energies derived from an analysis of unperturbed lines, i.e., the Q-branch transitions to the f Λ-doublet component of the $C^1\Pi$ state and the low J levels for the $B^1\Sigma^+$ state. The arrows represent the energy shift (cm^{-1}) of the observed energy levels from those calculated based on the molecular constants in Table II.

A full quantitative treatment of the perturbations in the HF and DF $B^1\Sigma^+$ and $C^1\Pi$ states was not undertaken. For a $^1\Sigma^+ - ^1\Pi$ spin-orbit interaction with off-diagonal elements of the form $\langle B^1\Sigma^+|H_{so}|C^1\Pi\rangle \propto B[J(J+1)]^{1/2}$, equal but opposite energy shifts for J levels of the $B^1\Sigma^+$ and $C^1\Pi$ states would be predicted (*19, 20*). However, Fig. 5 shows that this is not the case. The measured energy level shifts caused by the perturbation are larger in HF than in DF. This is in agreement with the spin-orbit interaction's dependence on the rotational constant, B, which is inversely proportional to the reduced mass. It was previously postulated that perturbations in the $B^1\Sigma^+$ state might also be caused by the $b^3\Pi$ state (*4, 21*). This state was observed in $b^3\Pi - X^1\Sigma^+$ XUV absorption (*4*), and also, very weakly, in the present 1 + 1 REMPI spectra. More spectroscopic information on this $b^3\Pi$ state will be required before a detailed multi-state deperturbation analysis can be attempted. The assumption of a sequence of avoided crossings between the B and C states gives us some qualitative understanding of these perturbations. More importantly, the observed spectral lines can be assigned unambiguously.

For the HF molecule, rotational constants for the $B^1\Sigma^+ v = 0$–10 and $v = 14$–73 vibronic levels were previously determined from B–X emission and absorption studies (*4*). The spectroscopy of the $B^1\Sigma^+$ state of DF is less well established. Johns and Barrow (*3*) first analyzed the $v = 0$ to 3 bands from VUV emission spectra. More recently, again observing VUV emission, Coxon and Hajigeorgiou (*9*) extended the

observation of the $B^1\Sigma^+$ state in DF to $v = 5$ and reported accurate rotational constants. In the present work we have investigated for the first time the absorption spectrum of DF in the range 101 000–106 000 cm^{-1}. For 14 consecutive vibrational levels of $B^1\Sigma^+$, denoted as $v = n + 27$ to $v = n + 40$, the B_v constants and the ν_0 values (band origins) are determined from least-squares fits to the observed line positions, using the Hamiltonian of Eq. (1). In this fit the upper state centrifugal distortion constant is fixed at 5×10^{-4} cm^{-1}, the same value as for the ground state. The results are listed in Table III. A definitive identification of the vibrational quantum numbering for this vibrational sequence cannot be given because information is missing about levels between $v = 5$ and $v = n + 27$. Figure 6 shows the spacing between the vibrational levels ΔG as a function of $v + \frac{1}{2}$. A smooth curve through the values for the lowest vibrational levels (*9*) and the present data leads us to estimate $-3 < n < 3$.

Figure 7 shows the rotational constant, B_v, as a function of v for the DF $B^1\Sigma^+$ state. The increase in the value of the rotational constant B_v for vibrational levels $v > n + 34$ signifies interaction between electronic states so that the effective mean internuclear distance decreases in the vibrational levels of the $B^1\Sigma^+$ higher than 104 000 cm^{-1}. In ab initio configuration interaction calculations, Bettendorf *et al.* (*22*) find a potential curve for the $B^1\Sigma^+$ state of HF/DF with a kink at the inner wall of the potential well. At an energy of about 12.8 eV above the ground state the slope of the inner well curve becomes less steep. This corresponds to a decrease of the internuclear distance, and it explains the observed increase in the rotational constant

TABLE III

Molecular Constants (in cm^{-1}) for the DF $B^1\Sigma^+$ State (The D Constant for This State Is Fixed at 5×10^{-4} cm^{-1}; the Cited Uncertainties Represent Two Standard Deviations; The Constants for $v = 0$ to $v = 5$ Are from Coxon and Hajigeorgiou (*9*) Where the D Constant Was Not Constrained)

v	B_v	ν_0
0	2.1152 (1)[a]	83 712.85 ± 0.2[b]
1	2.1077 (1)	84 534.61 ± 0.2
2	2.1001 (1)	85 338.04 ± 0.2
3	2.0923 (2)	86 123.53 ± 0.2
4	2.0840 (2)	86 891.67 ± 0.2
5	2.0754 (3)	87 642.70 ± 0.2
n+27	1.866 ± 0.003	101 082.21 ± 0.05
n+28	1.867 ± 0.003	101 531.06 ± 0.05
n+29	1.861 ± 0.002	101 970.93 ± 0.09
n+30	1.839 ± 0.001	102 401.68 ± 0.02
n+31	1.841 ± 0.001	102 823.40 ± 0.04
n+32	1.832 ± 0.002	103 236.35 ± 0.05
n+33	1.834 ± 0.003	103 640.60 ± 0.16
n+34	1.821 ± 0.002	104 036.33 ± 0.05
n+35	1.822 ± 0.002	104 423.56 ± 0.09
n+36	1.850 ± 0.017	104 802.11 ± 0.20
n+37	1.816 ± 0.012	105 172.48 ± 0.42
n+38	1.859 ± 0.002	105 534.10 ± 0.02
n+39	1.867 ± 0.003	105 887.51 ± 0.06
n+40	1.884 ± 0.003	106 232.44 ± 0.11

[a] Accuracy is reflected by the number of significant digits and the standard error is in parentheses.

[b] Relative accuracy is reflected by the number of significant digits, but absolute accuracy depends on $G''(16) + Y_{00} = 37\,776.9 \pm 0.2$ cm^{-1}, which is the energy of the $X\,^1\Sigma^+$ $v=16$ level with respect to the minimum of the $X\,^1\Sigma^+$ potential (J.A. Coxon, private communication).

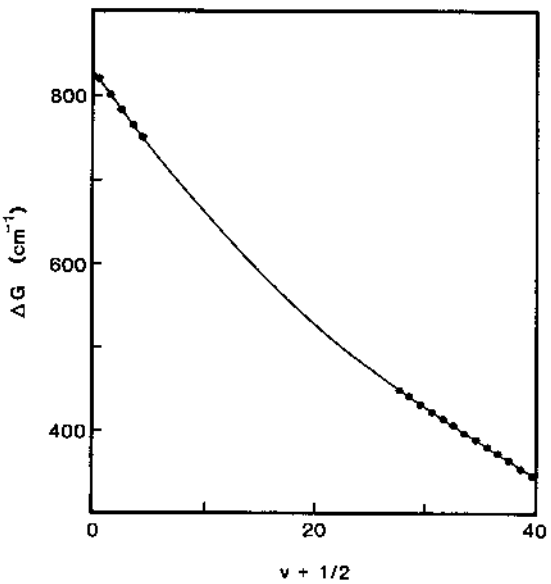

FIG. 6. The vibrational spacing ΔG for the DF $B^1\Sigma^+$ state as a function of $v + \frac{1}{2}$. The error in ΔG is ± 0.2 cm^{-1}. Values for $v = 0$–4 are taken from Coxon and Hajigeorgiou (*9*).

for $v > n + 34$ (see Fig. 7). We assume the potential curves for HF and DF to be identical. It follows that the change in the slope in the B state potential below 13 eV is caused by a mixing with a $^1\Sigma^+$ Rydberg state of the same symmetry, denoted by $^1\Sigma^+_{R1}$ by Bettendorf *et al.* (*22*). This state has a calculated minimum at 14 eV. It corresponds to a state denoted by $D^1\Sigma^+$ which was observed in $D^1\Sigma^+$–$X^1\Sigma^+$ transitions in HF in the region of 112 000 cm^{-1} (*7*).

Douglas and Greening (*7*) state that "many sharp well resolved lines showing no obvious band structure" in addition to the analyzed band systems occur in the range 66–100 nm. Over the small range covered in the present mass-selected spectroscopic study, 94.0–99.0 nm, no features that could not be assigned to B–X, C–X, and b–X (weak) transitions are observed.

B. Origin of H^+ and HF^+ Ion Production

As a general rule, we find that in 1 + 1 REMPI with the HF $C^1\Pi$ state as an intermediate, the ion yield is predominantly HF^+, while from ionization through the HF $B^1\Sigma^+$ state an appreciable amount of H^+ (on the order of 25–50%) is observed. We do not present a detailed quantitative analysis of the H^+/HF^+ ratio because the mass dependence of the ion detector response is not calibrated. Moreover, the H^+/HF^+ ratio is somewhat dependent on the voltage settings on the repeller, extractor, and ion steering plates. These trends are also observed in similar 1 + 1 REMPI studies of H_2 and F_2. After excitation of widely bound ionic states, such as the $H_2 B^1\Sigma^+_u$ $v = 13$–17 levels and the F_2 $C^1\Sigma^+_u$ and $D^1\Sigma^+_u$ states (*23*), H^+ and F^+ as well as H_2^+ and F_2^+ are produced. In contrast, after a first excitation step to a II state of Rydberg

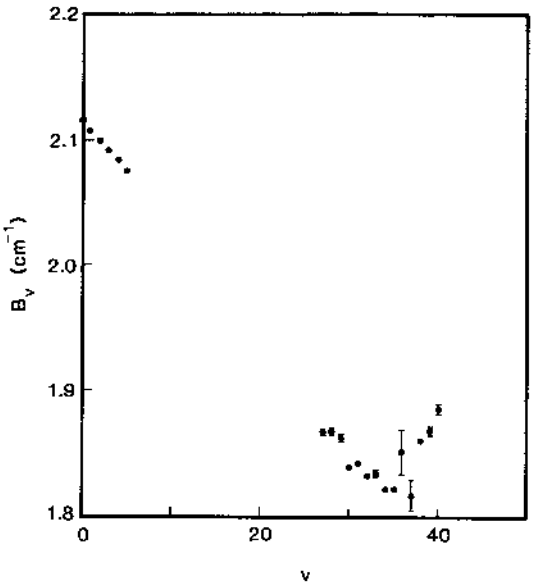

FIG. 7. The rotational constant B_v for different vibrational levels of the DF $B^1\Sigma^+$ state. The values for v = 0–4 are taken from Coxon and Hajigeorgiou (*9*).

character with a much smaller internuclear equilibrium distance, such as the H_2 $C^1\Pi_u$ v = 2–4 levels and the F_2 $H^1\Pi_u$ v = 0 and 1 levels, it is almost exclusively the parent ion that is formed.

From the one-photon ionization studies of Berkowitz *et al.* (*24*), the energy balance for the different ionization channels in HF/DF is known:

$$\begin{aligned}
HF + \Delta E &\rightarrow HF^+ + e^- && \Delta E = 16.007 \text{ eV}\\
HF + \Delta E &\rightarrow H^+ + F + e && \Delta E = 19.445 \text{ eV}\\
HF + \Delta E &\rightarrow H^+ + F^- && \Delta E = 15.994 \text{ eV}\\
DF + \Delta E &\rightarrow DF^+ + e^- && \Delta E = 16.030 \text{ eV}\\
DF + \Delta E &\rightarrow D^+ + F + e^- && \Delta E = 19.513 \text{ eV}\\
DF + \Delta E &\rightarrow D^+ + F^- && \Delta E = 16.064 \text{ eV}.
\end{aligned}$$

It is evident that parent ion formation and ion-pair production processes are energetically possible in a 1 XUV + 1 UV excitation scheme, even for excitation through the DF $B^1\Sigma^+ v = n + 27$ level, the lowest level used as an intermediate in this study.

However, there is serious doubt about the ion-pair channel being the cause for the strong H^+/D^+ yields. Ion-pair formation is known to be a weak process. In the direct one-photon ion-pair production process in H_2 (*25*), as well as in the 1 XUV +1 UV process ((*26*) and our own results), the cross section for the $H^+ + H^-$ channel is on the order of 0.1% of the total ionization cross section. In the specific case of $H^+ + F$

formation from HF, Berkowitz *et al.* (*24*) found that ion production through this channel is weak, except for a strong, sharp resonance at 16.1 eV. For a 1+1 process this would correspond to XUV absorption at 12.1 eV, which is below the excitation region used in the present study. Attempts to detect F^- ions were unsuccessful, while in the same setup strong negative ion signals (from $H_2 \rightarrow H^+ + H^-$) could be detected.

This leads to the conclusion that the strong H^+/D^+ signals are produced in a dissociative process. Energetically, this requires the absorption of two UV photons after excitation into the HF or DF $B^1\Sigma^+$ state by one XUV photon. H^+/D^+ can then be produced in two ways:

(1) The parent ion HF^+/DF^+, which is formed by a 1+1 process, is subsequently dissociated into $H^+/D^+ + F$. The dissociation energy of HF^+ is $D_0^0(HF^+) = 3.42$ eV (*27*). It is not known yet whether there exists a suitable repulsive state in HF^+ that might enhance this process.

(2) HF or DF is doubly excited by a 1+1 process into a Rydberg state of the neutral molecule above the ionization limit. This state is coupled to a repulsive potential with the asymptotic limit $H(n = 2) + F$ at about 16 eV. The metastable and long-lived Rydberg atom $H(n = 2)$ is then ionized by one UV photon.

Both channels are energetically possible. A determination of the relative importance of processes (1) and (2) could be performed by means of photoelectron spectroscopy. In the case of 3+1 REMPI in H_2 this has been demonstrated by Bonnie *et al.* (*28*).

C. *State-Specific Detection Sensitivity*

The 1 + 1 MPI scheme exploited in the present spectroscopic study may provide a viable technique for quantum-state-specific detection of HF (DF). Resonant excitation with XUV radiation in a one-photon step has the advantage that AC Stark and saturation effects in the spectra are avoided, in contrast to multiphoton excitation processes, where high power densities are required. Because of unfavorable Franck–Condon factors in the lowest part of the $B^1\Sigma^+$ potential well, a wavelength of ~200 nm or shorter is needed for 2+1 MPI detection of HF/DF. 3+1 and 2+1 multiphoton ionization in HF/DF have not been observed to date.

The detection sensitivity for HF for the strongest band observed, the C–X band, was found to be 10^7 molecules per cm^3 per quantum state. This limit was observed for tripling in N_2 with an incident UV energy of 6.0 mJ/pulse and a resolution of 1.2 cm^{-1}. To use this 1 XUV + 1 UV MPI technique to deduce meaningful rotational state populations, the wavelength dependence of both the HF^+/H^+ branching ratio and the ionization cross section from the $B^1\Sigma^+$ state must be characterized. The HF^+ and H^+ spectra for the $B^1\Sigma^+$ state of HF are nearly identical, indicating that any branching dependence on rotational level is low or absent. In particular, this can be seen for $B^1\Sigma^+ v = 30$ state in Fig. 1. Preliminary studies of the $B^1\Sigma^+ v = 31$ state allowed us to obtain a well behaved room temperature population distribution. Peak intensity measurements for P and R transitions originating from rotational states $J = 0$ to $J = 7$ were corrected for varying XUV power and transition moments and yielded a Boltzman population distribution with a temperature of $T = 304 \pm 13$ K.

This may be contrasted to the 2 + 1 REMPI detection of HCl (*29*), where anomalous line strengths for rotational transitions require correction factors up to a factor of 4.4 for $J = 7$ to extract rotational state populations. From our study we estimate that correction factors for 1 + 1 REMPI through the $B^1\Sigma^+ v = 31$ state of DF are less than 1.5 for $J = 0$, 1, 2, 3, 4, 6 and 7. Because of a large resonance in the Xe tripling curve near the $R(5)$ and $P(5)$ transitions, $J = 5$ was not included in the analysis. We conclude that 1 + 1 REMPI through the $B^1\Sigma^+$ state is a viable technique for state-selective detection of HF (DF).

ACKNOWLEDGMENTS

We thank Chifuru Noda for his help with the computer fitting of the spectra and Mark Buntine for his experimental assistance. We also appreciate the critical reading of a draft of this manuscript by John A. Coxon. This work was supported by the National Science Foundation under NSF PHY 85-06668.

RECEIVED: June 19, 1989

REFERENCES

1. R. S. MULLIKEN, *Phys. Rev.* **50,** 1017–1027 (1936).
2. R. S. MULLIKEN, *Phys. Rev.* **51,** 310–332 (1937).
3. J. W. C. JOHNS AND R. F. BARROW, *Proc. R. Soc. London Ser. A* **251,** 504–518 (1959).
4. G. DILONARDO AND A. E. DOUGLAS, *Canad. J. Phys.* **51,** 434–445 (1973).
5. D. E. MANN, B. A. THRUSH, D. R. LIDE, JR., J. J. BALL, AND N. ACQUISTA, *J. Chem. Phys.* **34,** 420–431 (1961).
6. D. W. WEBB AND K. NARAHARI RAO, *J. Mol. Spectrosc.* **28,** 121–124 (1968).
7. A. E. DOUGLAS AND F. R. GREENING, *Canad. J. Phys.* **57,** 1650–1661 (1979).
8. F. C. DELUCIA, P. HELMINGER, AND W. GORDY, *Phys. Rev. A* **3,** 1849–1857 (1971).
9. J. A. COXON AND P. G. HAJIGEORGIOU, *J. Mol. Spectrosc.* **133,** 45–60 (1989).
10. W. UBACHS, L. TASHIRO, AND R. N. ZARE, *Chem. Phys.* **130,** 1–13 (1989).
11. T. P. SOFTLEY, W. E. ERNST, L. M. TASHIRO, AND R. N. ZARE, *Chem. Phys.* **116,** 299–309 (1987).
12. F. HELLNER AND J. LUKASIK, *Opt. Commun.* **51,** 347–351 (1984).
13. S. GERSTENKORN AND P. LUC, "Atlas du spectroscopic de la molecule d'iode," C.N.R.S., Paris, 1978.
14. S. GERSTENKORN AND P. LUC, *Rev. Phys. Appl.* **14,** 791–794 (1979).
15. L. M. TASHIRO, W. UBACHS, M. A. BUNTINE, AND R. N. ZARE, unpublished results.
16. R. H. PAGE, R. J. LARKIN, A. H. KUNG, Y. R. SHEN, AND Y. T. LEE, *Rev. Sci. Instrum.* **58,** 1616–1620 (1987).
17. J. A. R. SAMSON, "Techniques of Vacuum Ultraviolet Spectroscopy," Pied, Lincoln, Nebraska, 1969.
18. D. A. JENNINGS AND J. S. WELLS, *J. Mol. Spectrosc.* **130,** 267–268 (1988).
19. I. KOVAĆS, "Rotational Structure in the Spectra of Diatomic Molecules," Hilger, London, 1969.
20. H. LEFEBVRE-BRION AND R. W. FIELD, "Perturbations in the Spectra of Diatomic Molecules," Academic Press, New York, 1986.
21. G. A. SEGAL AND K. WOLF, *Chem. Phys.* **56,** 321–326 (1981).
22. M. BETTENDORF, R. J. BUENKER, S. D. PEYERIMHOFF, AND J. ROEMELT, *Z. Phys. A* **304,** 125–135 (1982).
23. L. M. TASHIRO, W. UBACHS, AND R. N. ZARE, unpublished results.
24. J. BERKOWITZ, W. A. CHUPKA, P. M. GUYON, J. H. HOLLOWAY, AND R. SPOHR, *J. Chem. Phys.* **54,** 5165–5180 (1971).
25. W. A. CHUPKA, P. M. DEHMER, AND W. T. JIVERY, *J. Chem. Phys.* **63,** 3929–3944 (1975).
26. R. H. PAGE, R. J. LARKIN, Y. R. SHEN, AND Y. T. LEE, *Phys. Rev. Lett.* **56,** 328–331 (1986).
27. J. BERKOWITZ, *Chem. Phys. Lett.* **11,** 21–26 (1971).
28. J. H. M. BONNIE, J. W. J. VERSCHUUR, H. J. HOPMAN, AND H. B. VAN LINDEN VAN DEN HEUVELL, *Chem. Phys. Lett.* **130,** 43–48 (1986).
29. T. A. SPIGLANIN, D. W. CHANDLER AND D. H. PARKER, *Chem. Phys. Lett.* **137,** 414–420 (1987).